Journal of Applied Physics ARTICLE scitation.org/journal/jap

Germanium doping of cubic GaN grown by molecular beam epitaxy

Cite as: J. Appl. Phys. **125**, 095703 (2019); doi: 10.1063/1.5066095
Submitted: 12 October 2018 · Accepted: 19 February 2019 ·
Published Online: 6 March 2019

View Online

Export Citation

CrossMark

M. Deppe,[1,a)] J. W. Gerlach,[2] S. Shvarkov,[1] D. Rogalla,[3] H.-W. Becker,[3] D. Reuter,[1] and D. J. As[1]

AFFILIATIONS

[1]Department Physik, Universität Paderborn, Warburger Str. 100, 33098 Paderborn, Germany
[2]Leibniz-Institut für Oberflächenmodifizierung (IOM) e.V., Permoserstr. 15, 04318 Leipzig, Germany
[3]RUBION, Ruhr-Universität Bochum, Universitätsstr. 150, 44801 Bochum, Germany

[a)]**Electronic mail:** michael.deppe@uni-paderborn.de

ABSTRACT

We present a study of germanium as an alternative to silicon for n-type doping of cubic GaN. We find that Ge is a well-suited donor impurity. Our layers were grown by plasma-assisted molecular beam epitaxy on 3C-SiC/Si (001) substrates. Germanium-doped layers were fabricated with donor concentrations ranging over several orders of magnitude up to $3.7 \times 10^{20}\,\mathrm{cm}^{-3}$. For comparison, silicon-doped layers with donor concentrations of up to $3.8 \times 10^{19}\,\mathrm{cm}^{-3}$ were also grown. Incorporation of germanium into the cubic GaN layers was verified by time-of-flight secondary ion mass spectrometry. The crystalline quality of our layers was analyzed using high-resolution x-ray diffraction. Germanium- as well as silicon-doped layers with donor concentrations above $10^{19}\,\mathrm{cm}^{-3}$ exhibited an increase of the dislocation density with increasing dopant concentration. The surface topography of our layers was investigated by atomic force microscopy. Comparable values for the surface roughness were measured for germanium- as well as silicon-doped layers. Optical properties were investigated by photoluminescence spectroscopy at 13 K. Doping with silicon resulted in a spectrally slightly narrower luminescence than doping with germanium. Donor concentrations and carrier mobilities were determined by Hall effect measurements at room temperature and we observe 20% higher electron mobilities for Ge-doping compared to Si-doping in the case of high dopant concentrations.

Published under license by AIP Publishing. https://doi.org/10.1063/1.5066095

I. INTRODUCTION

GaN-based optoelectronic devices are mostly grown in the thermodynamically stable hexagonal wurtzite crystal structure along the c-direction. Due to symmetry reasons, spontaneous and piezoelectric polarization fields are existent and limit the recombination efficiency in, e.g., double heterostructures or quantum wells. There exist several approaches to overcome these effects. One of them is to grow the metastable cubic zinc blende phase of GaN, where the aforementioned polarization fields are missing.

For device fabrication, it is essential to control p- and n-type doping of the semiconductor. Up to now, n-type doping of cubic GaN (c-GaN) is preferably realized by the incorporation of silicon.[1–4] It is well known that the incorporation of silicon in wurtzite GaN leads to tensile strain,[5] whereas it has recently been shown that this is not the case for the incorporation of germanium, allowing to grow highly doped layers with improved crystalline quality.[6]

Recently, we have demonstrated the incorporation of germanium into c-GaN layers grown by molecular beam epitaxy (MBE) and have presented first investigations of structural[7] and optical properties.[8] In this paper, we provide an extensive study on the structural, electrical, and optical properties of germanium doped c-GaN and give a comparison to silicon doped layers.

II. EXPERIMENTAL DETAILS

Our c-GaN layers were grown by plasma-assisted molecular beam epitaxy (MBE) in a *Riber*-32 system equipped with an *Oxford Applied Research* HD25 radio frequency plasma source to supply activated nitrogen atoms. Not intentionally doped (n.i.d.), germanium-doped, and silicon-doped c-GaN layers were grown. To cover a large range of doping densities, the germanium effusion cell temperature was varied in a range of 600 °C to 1000 °C. The silicon effusion cell was operated at temperatures from 950 °C and the maximum temperature reached was 1100 °C. The layers were deposited on 3C-SiC/Si (001) substrates at a growth temperature of 720 °C. A gallium beam equivalent pressure (BEP) of 1.1×10^{-7} Torr and a nitrogen flow of 0.21 sccm were employed for all layers.

Published under license by AIP Publishing.

TABLE I. Overview of doping characteristics and basic sample properties.

Dopant	Cell temp. (°C)	Flux ($cm^{-2} s^{-1}$)	Estimated donor concentration (cm^{-3})[a]	TOF-SIMS donor concentration (cm^{-3})	Carrier mobility ($cm^2 V^{-1} s^{-1}$)	Thickness (nm)
n.i.d.[b]						612
Ge	600	1.8×10^6	*1.7×10^{14}*	1.5×10^{18}		588
Ge	650	3.1×10^7	*3.0×10^{15}*			552
Ge	700	3.4×10^8	*3.2×10^{16}*	3.6×10^{18}		556
Ge	750	3.3×10^9	*3.1×10^{17}*			558
Ge	800	2.9×10^{10}	*2.7×10^{18}*	6.0×10^{18}	105	543
Ge	900	9.3×10^{11}	**8.7×10^{19}**	7.7×10^{19}	90	460
Ge	1000	8.9×10^{12}	**3.7×10^{20}**	3.2×10^{20}	63	363
Si	950	1.1×10^{10}	*3.0×10^{17}*			607
Si	1000	6.2×10^{10}	*1.7×10^{18}*		84	647
Si	1050	2.8×10^{11}	*7.6×10^{18}*		74	611
Si	1100	1.4×10^{12}	**3.8×10^{19}**		77	564

[a]The donor concentrations of the two highest germanium-doped samples and the highest silicon-doped sample (bold) are determined by Hall effect measurements. Donor concentrations of lower doped samples were extrapolated based on the dopants vapor pressure curves. The extrapolated values are printed in italics. The GaN layer thickness was measured by reflectivity after growth.
[b]Not intentionally doped.

Reflection high energy electron diffraction (RHEED) was employed for *in situ* growth control.[9] After growth, the c-GaN layer thickness was determined by reflectometric interference spectroscopy. Time-of-flight secondary ion mass spectrometry (TOF-SIMS) was performed with an *ION-TOF* TOF-SIMS 5 instrument to analyze the composition of our layers. A primary ion beam of 15 keV $^{69}Ga^+$ ions scanned a $50 \times 50\,\mu m^2$ area. Depth profiling was done using a 1.0 keV Cs^+ beam covering an area of $300 \times 300\,\mu m^2$. Negative ion mass spectra were collected. To determine the dislocation density and the amount of hexagonal inclusions, high-resolution x-ray diffraction (HRXRD) was carried out on a *Philips* X'Pert MRD. The surface topography of our layers was investigated using a *Nanosurf* Mobile S atomic force microscope (AFM) operating in contact mode. Photoluminescence (PL) spectra were taken using a continuous wave frequency-quadrupled Nd:YAG laser (266 nm) operating at a power of 5 mW as an excitation source. An *Andor* iDus 420 CCD detector array mounted on a *SPEX* 270 M imaging spectrograph was used for light detection. Carrier density and mobility were determined by Hall effect measurements in van der Pauw geometry at room temperature.

III. RESULTS AND DISCUSSION

The basic layer properties and effusion cell temperatures, which were used to achieve different doping levels, are summarized in Table I. The donor concentrations were taken from Hall effect measurements, assuming the two highest germanium-doped layers and the highest silicon-doped layer to be degenerate. In this case, the measured carrier density is equal to the donor concentration. Donor concentrations of lower doped layers were extrapolated based on the dopants vapor pressure curves.[10,11] Since germanium has a significantly higher vapor pressure compared to silicon, it is possible to achieve a two orders of magnitude higher doping level for comparable effusion cell temperatures.

A. TOF-SIMS-measurements

The germanium-doped c-GaN samples were investigated by TOF-SIMS to gain depth-resolved information on the Ge incorporation into the cubic GaN epilayers. To obtain absolute values for the germanium concentration, a calibration of the germanium-related secondary ion signals needs to be done. Therefore, we fabricated and analyzed ion-implanted samples, which will be discussed in the following.

Germanium ions were implanted into 580 nm thick not intentionally doped (n.i.d.) c-GaN layers by two different ion implanters at the Ruhr-University of Bochum. The first implanter (100 kV ion accelerator) with low ion energies of 95 keV allows shallow implantation and uses ^{72}Ge, whereas the second implanter (4 MV tandem accelerator) with high ion energies of 750 keV allows deep implantation and uses ^{74}Ge. In addition, the two different Ge isotopes result in two independent TOF-SIMS signals, which can be used for analysis.

The implantation parameters chosen are depicted in Table II. The germanium fluences resulted in volume concentrations between about 10^{18} and $10^{20}\,cm^{-3}$. These Ge concentrations are similar to those intended to be incorporated during MBE growth. The implantation profiles (Ge ions per fluence) in cubic GaN are simulated by the freeware software package SRIM-2013 (*SRIM—The Stopping*

TABLE II. Parameters for implantation of Ge ions into c-GaN layers.

Implantation sample	Isotope	Ion energy (keV)	Fluence (cm^{-2})	Angle of incidence (deg)
A	^{72}Ge	95	1.6×10^{15}	7
B	^{74}Ge	750	1.0×10^{15}	7
C	^{74}Ge	750	1.0×10^{14}	7

Published under license by AIP Publishing.

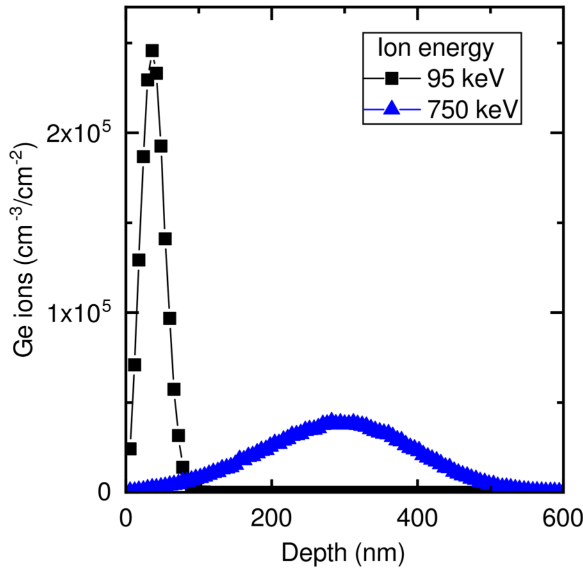

FIG. 1. Implantation profiles (Ge ions per fluence) of Ge in cubic GaN simulated by SRIM-2013 for an angle of incidence of 7° and different ion energies of 95 keV and 750 keV, respectively.

and Range of Ions in Matter, Ref. 12) and are shown in Fig. 1 for different ion energies of 95 keV and 740 keV, respectively. The Germanium concentrations are obtained by multiplying the implantation profiles with the respective fluence.

In Fig. 2, the germanium depth profiles of ion-implanted samples measured by TOF-SIMS are shown together with the respective GaN^- signal. As for the GaN layer, the sputtering time is proportional to the depth the signals originate from. The transition between the GaN layer and 3C-SiC substrate occurs after approximately 1050 s of sputtering. For the implanted sample A, two signals that are related to the implanted ^{72}Ge ions were recorded. The $^{72}Ge^-$ signal is directly related to the implanted ions, but also the $^{72}GeN^-$ signal reflects the germanium depth profile. However, the $^{72}GeN^-$ signal features a higher sensitivity, but it is overlapped by a GaN-related signal (the $^{72}GeN^-$ signal is also present in undoped layers). For the implanted sample B, two signals that are related to the implanted ^{74}Ge ions were recorded. Again, the $^{74}GeN^-$ signal features a higher sensitivity in comparison to pure $^{74}Ge^-$, and in contrast to the $^{72}GeN^-$ signal, it is not overlapped by another mass signal.

For calculating the absolute germanium concentration, the $^{74}GeN^-$ signal from the implanted samples B and C is taken. In the case of the implanted sample A, the constant GaN-related background is subtracted from the $^{72}GeN^-$ signal. The remaining intensity is corrected by the isotopic ratio of germanium to obtain a signal that is adequate to the $^{74}GeN^-$ signal in samples B and C. In the next step, the $^{74}GeN^-$ signals are normalized to the respective GaN^- signal intensity to take varying ion beam currents or sputter parameters into account. At last, the maxima of the simulated implantation profiles (multiplied by the fluence) and the maxima of the implantation profiles measured by TOF-SIMS are correlated. In Fig. 3, the maximum ^{74}Ge concentration is plotted versus the intensity ratio of the $^{74}GeN/^{69}GaN$ mass signal maximum. From the linear regression of the three pairs of data, a linear equation for calibration is obtained and a proportionality factor of $k = 1.5695 \times 10^{21}\ cm^{-3}$ is estimated. The TOF-SIMS measurements for the MBE-grown samples are discussed in the next paragraph.

Figure 4 shows the TOF-SIMS depth profile of the layer with an estimated germanium density of $2.7 \times 10^{18}\ cm^{-3}$ ($T_{Ge} = 800\ °C$). After a sputter time of approximately 860 s, a significant change of the recorded depth profile can be observed, indicating that the interface between the GaN layer and the 3C-SiC substrate is reached at this point. For the other layers with different thicknesses, the time required until the interface is reached linearly scales with the layer thickness. The predominant negative secondary ion signals from the c-GaN layer originate from GaN^- and GaO^- ions. Two signals, originating from $^{74}Ge^-$ and $^{74}GeN^-$ ions, prove the incorporation of germanium into the GaN layer. Furthermore, several other germanium isotopes (^{70}Ge, ^{72}Ge, ^{73}Ge, and ^{76}Ge)

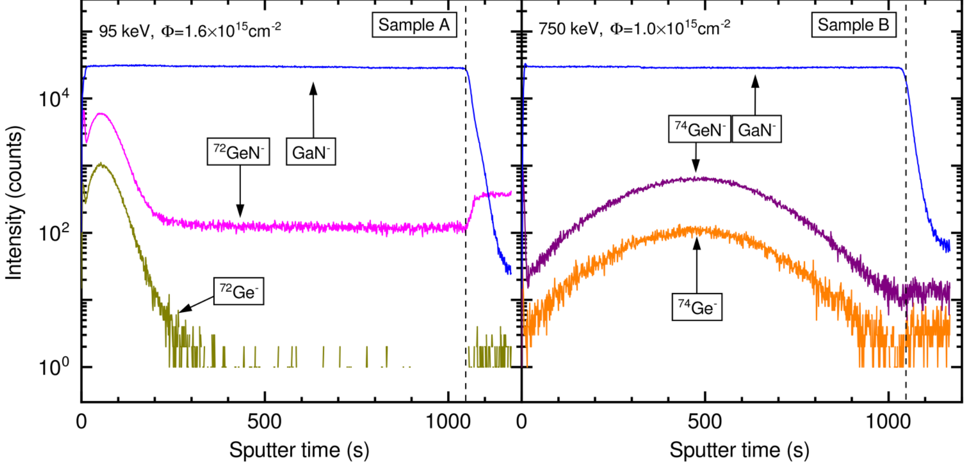

FIG. 2. Ge depth profiles of the ion-implanted samples, measured by TOF-SIMS.

Published under license by AIP Publishing.

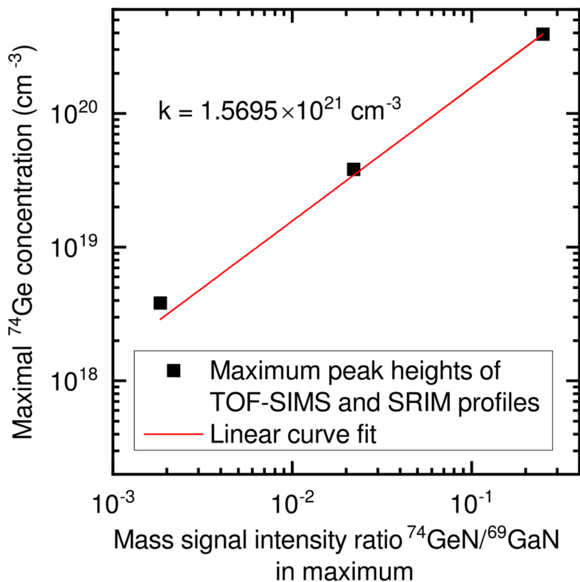

FIG. 3. Maximal ^{74}Ge concentration (maximum of SRIM calculation multiplied with implantation fluence) versus mass signal intensity ration ^{74}GeN/^{69}GaN in maximum.

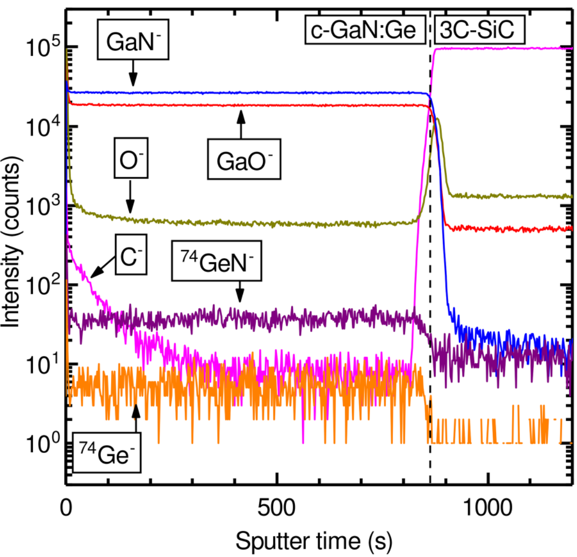

FIG. 4. TOF-SIMS depth profile of a germanium-doped c-GaN layer with a doping density of 2.7×10^{18} cm^{-3} ($T_{Ge} = 800$ °C). Reproduced with permission from Deppe *et al.*, Phys. Status Solidi B **254**, 1600700 (2017). Copyright 2017 WILEY-VCH Verlag GmbH & Co. KGaA, Weinheim. Some labels are changed from the original publication for better clarity.

could be found in our layers, but for the sake of clarity, the corresponding signals are not shown here. Both ^{74}Ge$^-$ and ^{74}GeN$^-$ signals proceed proportionally to each other, with ^{74}GeN$^-$ offering the advantage of approximately six times higher sensitivity. Therefore, we preferentially take the ^{74}GeN$^-$ signal as an indicator for germanium incorporation. With the calibration done in the paragraph above and taking into account the natural abundance of ^{74}Ge (36.7%[13]), we determine a germanium concentration of 6.0×10^{18} cm^{-3} in this layer. This value is approximately larger by a factor of two than the germanium concentration estimated based on the vapor pressure curve. The germanium concentrations of the other layers determined by TOF-SIMS are listed in Table I. In addition, we see that C and O are incorporated into the c-GaN layers, most likely originating from the residual gas (mainly H_2O, CO_2, CO, and hydrocarbons) in the growth chamber. C and O are known to form acceptors and donors in GaN, respectively.[1,14] While all other signals remain constant throughout the entire GaN layer, the intensities of the C$^-$ and O$^-$ signals rise towards the surface. This effect is much more pronounced for the C$^-$ signal compared to the O$^-$ signal.

B. Structural properties

Reflectometric interference spectroscopy measurements reveal layer thicknesses around 600 nm for all but the two highest germanium-doped layers (see Table I). These two layers exhibit a significantly lower thickness, although growth time was identical for all layers. A possible explanation for this growth rate reduction is the accumulation of germanium atoms on top of the surface during growth.[7] Impinging Ga and/or N atoms could be hindered from reaching the growth front by these excess germanium atoms. Germanium could act as an antisurfactant as it is known for silicon in wurtzite GaN growth.[15] On the other hand, it is reported that germanium acts as a surfactant in a-plane growth of wurtzite GaN at doping levels above 10^{20} cm^{-3}.[16] Further investigation on the role of silicon and germanium in c-GaN growth kinetics is required at this point.

HRXRD rocking curves of the (002) reflections were acquired to determine the dislocation density as a measure of the crystalline quality of our layers. According to Gay *et al.*,[17] the dislocation density D can be estimated from the rocking curve full width at half maximum (FWHM) $\Delta\theta$ by

$$D = \frac{\Delta\theta^2}{9b^2}, \qquad (1)$$

with b being the length of the Burgers vector. For 60° dislocations in the zinc blende structure, the length of the burgers vector is given by[18] $b = a/\sqrt{2}$ with $a = 4.503$ Å being the lattice constant of c-GaN.[19] In Fig. 5, the rocking curve FWHM $\Delta\theta$ and the calculated dislocation densities are plotted versus the donor concentration. Up to a donor concentration of 2.7×10^{18} cm^{-3}, $\Delta\theta$ of the germanium-doped layers stay at the level of the n.i.d. layer. With further increasing doping, a deterioration of $\Delta\theta$ can be observed, and for the highest germanium-doped layer, a four times higher rocking curve FWHM than for the n.i.d. layer is measured.

According to Ref. 20, due to the annihilation of dislocations, the dislocation density D is inversely proportional to the layer

Published under license by AIP Publishing.

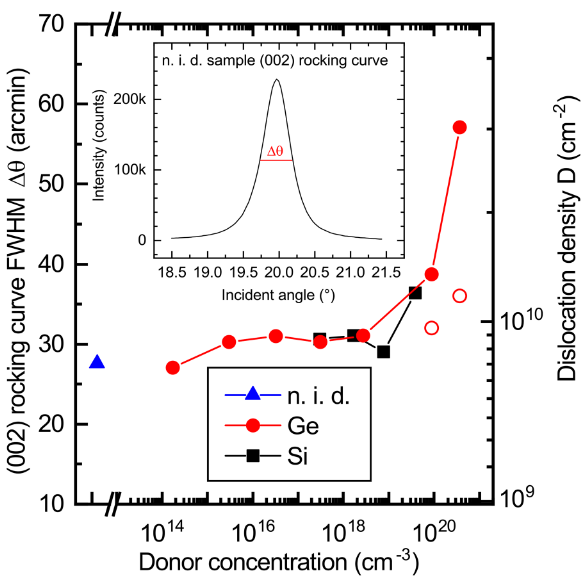

FIG. 5. HRXRD rocking curve FWHM of the c-GaN (002) reflection plotted versus the donor concentration of germanium-doped (full red circles) and silicon-doped (full black squares) layers. The n.i.d. layer is depicted by a full triangle. The corresponding dislocation density is calculated from the FWHM using Eq. (1). The open circles show to which extent the dislocation density of the two highest doped layers would have increased only due to their reduced layer thickness. The inset shows the rocking curve of the n.i.d. sample.

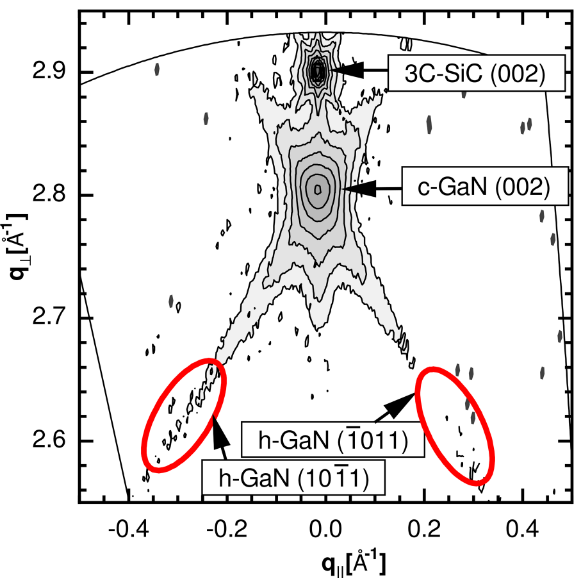

FIG. 6. A reciprocal space map (RSM) around the (002) reflection of the 3.7 × 10^{20} cm^{-3} germanium-doped layer. The positions where hexagonal inclusions are expected in c-GaN are marked by ellipses. No hexagonal inclusions are found in this Ge-doped c-GaN layer.

thickness d. We found a $D \propto d^{-0.5}$ correlation for c-GaN on 3C-SiC.[21] To rule out that the increased dislocation density of the two highest germanium-doped layers is based solely on the lower layer thickness, the mean dislocation density of 600 nm thick n.i.d. layers is taken to calculate the expected values for 460 nm and 363 nm thick layers. These values are plotted as open circles in Fig. 5. It is obvious that the degraded crystal quality is also caused by the doping and is not solely a result of the smaller layer thickness.

Comparing the germanium-doped to the silicon-doped layers, no significant difference in dislocation density can be found; merely, the $7.6 \times 10^{18}\,cm^{-3}$ silicon-doped layer exhibits a slightly lower dislocation density than the nearest lower doped layer. This may be explained by tensile strain that is induced by the incorporation of silicon. The tensile stain counteracts the compressive strain which is caused by the lattice mismatch of c-GaN to the 3C-SiC substrate. Romano *et al.*[5] reported for wurtzite GaN that the residual strain vanishes at a certain silicon doping level. We assume that the considered layer features very low residual strain and thus exhibits a lower dislocation density.

In Fig. 6, the (002) reciprocal space map (RSM) of the $3.7 \times 10^{20}\,cm^{-3}$ germanium-doped layer is plotted. The 3C-SiC (002) and the c-GaN (002) reflections are visible at $q_\perp = 2.9\,Å^{-1}$ and $q_\perp = 2.8\,Å^{-1}$, respectively. Hexagonal inclusions in c-GaN mainly grow on (111) facets.[21] If hexagonal inclusions are present, their $(10\bar{1}1)$ and $(\bar{1}011)$ reflections appear in reciprocal space maps (RSMs) of the (002) Bragg reflections.[21,22] Two ellipses indicate the areas where the reflections of hexagonal inclusions would appear. No peaks are visible in this range, indicating the amount of hexagonal inclusions in this sample is below the detection limit of around 1%. Also, none of the other layers discussed in this paper exhibit detectable hexagonal inclusions.

Atomic force microscope (AFM) measurements are performed on a $10\,\mu m \times 10\,\mu m$ area to characterize the surface topography of the layers. The surface quality is quantified by calculating the root mean square surface roughness S_q. The S_q values determined for various n.i.d., Ge-, and Si-doped layers are plotted in Fig. 7(a). The roughness of germanium-doped layers ranges between about 5 nm to 6 nm and thus is similar to that of the Si-doped and n.i.d. layers. Merely, the $8.7 \times 10^{19}\,cm^{-3}$ Ge-doped layer features a significantly lower roughness of about 2.4 nm. Si-doped layers show a reduced roughness in the $10^{19}\,cm^{-3}$ range. In Fig. 7(b), the AFM image of the highest Ge-doped layer is displayed. An accumulation of material along distinct lines can be seen. These lines most likely are antiphase domain boundaries, which have been observed previously on n.i.d. c-GaN layers.[23] The excess material along these boundaries is only present on the two highest Ge-doped layers. Not intentionally doped layers, Si-doped layers, and layers with lower Ge-doping do not show this feature. This supports the above-mentioned assumption of a germanium-accumulation during growth.

C. Electrical properties

Room temperature Hall effect measurements in van der Pauw geometry are performed to determine the carrier density and Hall mobility of our doped layers. Small indium beads are alloyed into the c-GaN layers at 420 °C for 5 min to fabricate ohmic contacts.

Published under license by AIP Publishing.

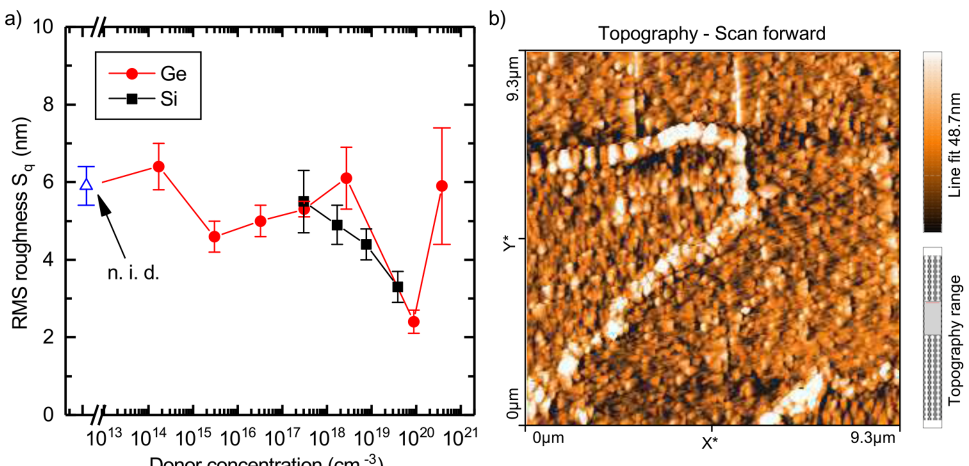

FIG. 7. (a) Root mean square surface roughness of Ge- and Si-doped c-GaN layers determined by AFM, depending on the donor concentration. (b) AFM image of the surface of the $3.7 \times 10^{20}\,cm^{-3}$ Ge-doped layer.

The 3C-SiC substrate shows n-type conductivity with a carrier density of $1.6 \times 10^{16}\,cm^{-3}$. For c-GaN epilayers with high doping levels, we expect that the current in the sample flows mainly through the c-GaN layer and the current flow through the 3C-SiC substrate can be neglected.

The n.i.d. c-GaN layer is found to show p-type conductivity with a hole concentration of $4.7 \times 10^{16}\,cm^{-3}$. In c-GaN, 60° dislocations are electrically active by trapping electrons, and thus they act as acceptors.[18,24] For the two highest germanium-doped layers and the highest silicon-doped layer, the c-GaN samples are expected to degenerate. In these cases, the measured electron concentrations equal the donor concentrations. The measured donor concentrations are listed in Table I. The highest donor concentration in the silicon-doped sample series is $3.8 \times 10^{19}\,cm^{-3}$ and was achieved using a cell temperature of 1100 °C. With germanium doping, the highest donor concentration we measured was $3.7 \times 10^{20}\,cm^{-3}$ for a cell temperature of 1000 °C. The layer grown with a silicon effusion cell temperature of 1000 °C features a two orders of magnitude lower donor concentration, due to the lower vapor pressure of Si.

Additionally, we measured the carrier mobility of the high-doped layers (Fig. 8 and Table I). The highest mobility we achieved with germanium doping was $105\,cm^2\,V^{-1}\,s^{-1}$, whereas the highest mobility of silicon-doped layers was $84\,cm^2\,V^{-1}\,s^{-1}$. Overall, the germanium-doped layers exhibit a carrier mobility about 20% higher than that of silicon-doped layers. The reduction of the electron mobility at higher doping levels can be explained by increased scattering at impurities. This effect is also observed in h-GaN and has been described theoretically.[25]

D. Optical properties

The PL spectra of the germanium-doped layers at 13 K are shown in Fig. 9. The individual peaks are identified exemplarily in Fig. 9(b) for the $3.2 \times 10^{16}\,cm^{-3}$ doped layer. The dashed vertical line marks the 13 K bandgap energy $E_G = 3.2928$ eV of c-GaN.[26,27] Emission above this energy originates from small hexagonal inclusions of wurtzite GaN whose bandgap energy is slightly larger. Three emission bands dominate the spectrum and are fitted by Gaussian functions. The emission at 3.2549 eV is related to the recombination of bound excitons (BX)[28,29] and features a FWHM of 36 meV. The highest intensity peak at 3.1733 eV originates from recombination of donor-acceptor pairs (D^0,A^0).[28] A further donor-acceptor pair recombination $(D^0,A^{0\prime})$ can be seen at 3.0784 eV. It is assumed that C is involved as an acceptor in this transition.[1,30] Luminescence below 3 eV is related to transitions involving deep defects, possibly N vacancies acting as deep donors.[2] Figure 9(a) shows the normalized and vertically shifted spectra of layers with different germanium concentrations. It is expected that with increasing doping level, the intensity of the donor-acceptor pair recombination becomes stronger compared

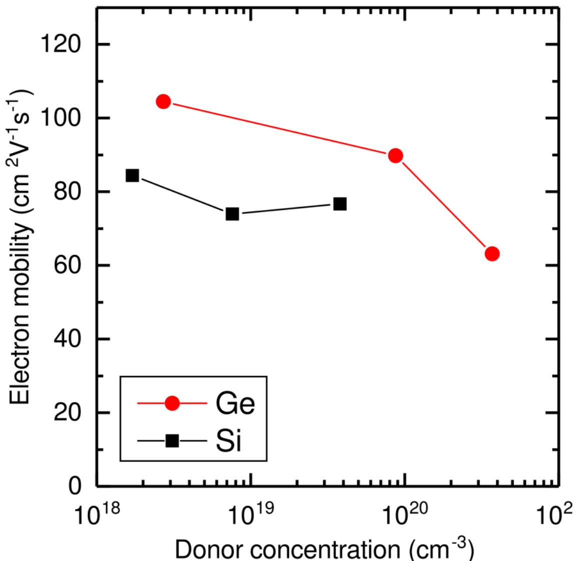

FIG. 8. Carrier mobility of the high-doped c-GaN layers determined by Hall effect measurements at room temperature.

Published under license by AIP Publishing.

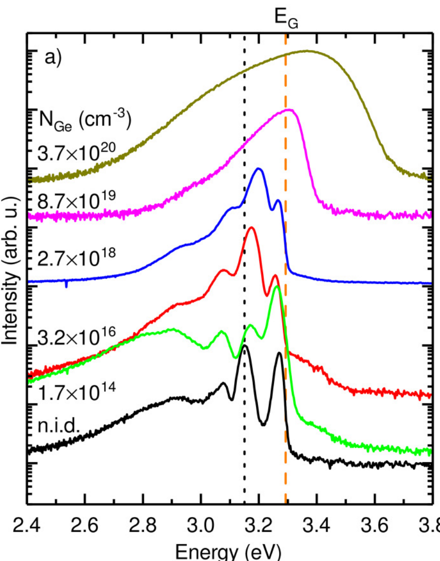

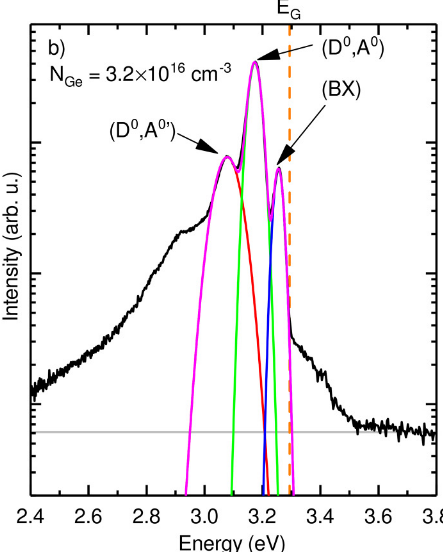

FIG. 9. (a) The 13 K PL spectra of Ge-doped layers and the not intentionally doped layer. The spectra are normalized and shifted vertically for better clarity. (b) Gaussian functions are fitted to the PL spectrum of the 3.2×10^{16} cm^{-3} Ge-doped layer. The near band edge emission consists of the recombination of bound excitons (BX) and two donor-acceptor pair transitions (D^0,A^0) and (D^0,$A^{0\prime}$). The horizontal solid line visualizes the constant background signal of the CCD detector. Reproduced with permission from As *et al.*, MRS Adv. **2**, 283 (2017). Copyright 2016 Materials Research Society.

to the (BX) intensity. The opposite effect is noticed when comparing the n.i.d. layer and the 1.7×10^{14} cm^{-3} doped layer. Thus, we conclude that in both these layers, the doping level is dominated by the unintentional incorporation of residual oxygen. In the 3.2×10^{16} cm^{-3} doped layer, the (D^0,A^0) emission becomes more intense and exhibits a larger intensity than the (BX) peak. A blue shift of the (D^0,A^0) emission can be observed with increasing donor concentration, which is due to the Coulomb interaction of donors and acceptors.[31] With further increased doping, the peaks merge and spectral broadening occurs, indicating degenerate doping. The 3.7×10^{20} cm^{-3} doped layer shows emission far beyond the bandgap energy which is furthermore caused by the Burstein-Moss effect. A more detailed report on the optical properties of germanium-doped layers can be found in Ref. 8.

In Fig. 10, the PL spectra of germanium- and silicon-doped layers with almost identical dopant concentrations are plotted. The (D^0,A^0) emission is dominating in both spectra and features a comparable intensity in both cases. However, the emission peaks of the silicon-doped layer exhibit slightly smaller spectral broadening. The FWHM of the (D^0,A^0) peak in the spectrum of the germanium-doped layer is 62 meV, whereas in the case of silicon doping, it is 50 meV. The narrower PL-linewidth of the Si doped sample may be explained by the larger epilayer thickness of Si-doped sample (647 nm) in comparison to the Ge-doped sample (543 nm). In the Ge-doped sample, the slightly higher dislocation density may contribute to increased scattering, which may cause the linewidth broadening.

E. Incorporation efficiency

Comparing the vapor pressure curves of germanium[10] and silicon[11] in the temperature range used for high doping, the vapor pressure of germanium is found to be approximately three orders of magnitude higher than that of silicon. The measured donor concentrations of germanium-doped layers by contrast are two orders of magnitude higher than those of silicon-doped layers with equal dopant cell temperature. Thus, we estimate a 10 times lower incorporation efficiency of germanium compared to silicon.

The incorporated donor concentrations of the germanium-doped layers determined by TOF-SIMS, PL, and Hall-effect measurements are plotted versus the effusion cell temperature in Fig. 11. Additionally, the vapor pressure curve of germanium[10] is also depicted in Fig. 11 as a full red curve. The vapor pressure

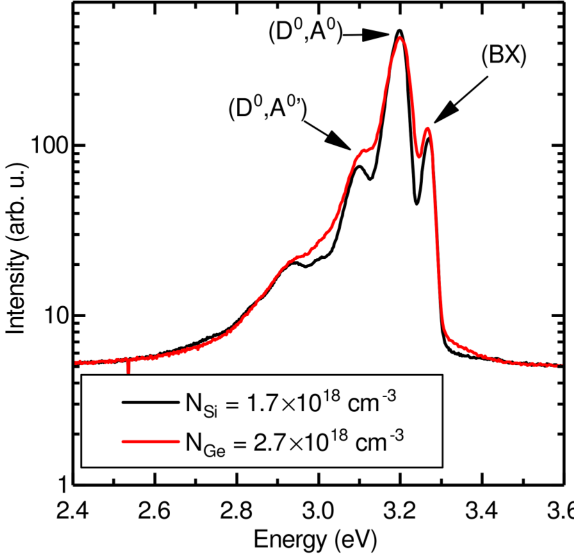

FIG. 10. Comparison of the 13 K PL spectra of two c-GaN epilayers doped by Ge and Si with comparable donor concentration.

Published under license by AIP Publishing.

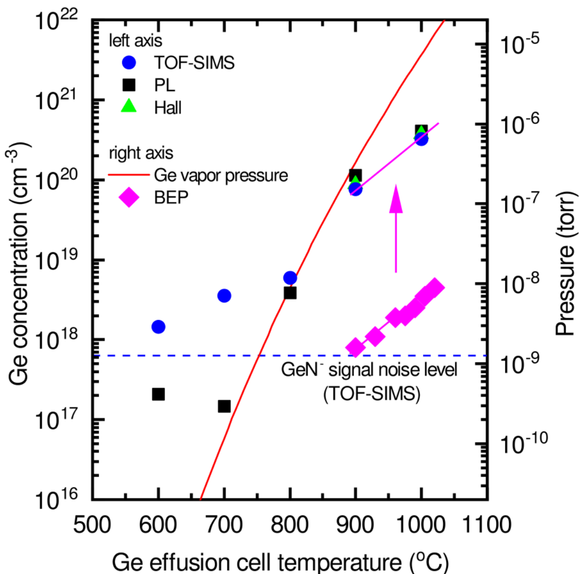

FIG. 11. Donor concentrations of the Ge-doped layers are determined by TOF-SIMS, PL, and Hall effect measurements. The dashed line indicates the noise level of the GeN^- signal, which limits the detection of Ge in TOF-SIMS. The vapor pressure curve of Ge is overlaid to fit the measured concentrations. In addition, the measured beam equivalent pressure (BEP_{Ge}) of the Ge effusion cell is plotted. A line is fitted to the BEP data and shifted towards the donor concentration data as a guide to the eye.

curve is obtained by fitting Eq. (2)[32] to the vapor pressure data from Ref. 10,

$$\log(p) = -\frac{A}{T} + B + C \cdot \log(T). \tag{2}$$

If p is given in Torr and T is the temperature in °C, the fitted constants A, B, and C are 4311, −58.06, and 19.08 for Ge, respectively.

From PL measurements, the donor concentration has been calculated from the shift of the transition energy E_{DA} of the donor-acceptor pair recombination[31] (D^0,A^0)

$$E_{DA} = E_G - (E_A + E_D) + \frac{e^2}{4\pi\varepsilon_0\varepsilon_r r}, \tag{3}$$

with $E_A = 130$ meV for the acceptor binding energy, $E_D = 30$ meV for the donor binding energy, $\varepsilon_r = 9.44$ the relative permittivity of c-GaN, and r is the mean distance of acceptors to donors,[26]

$$r = \sqrt[3]{\frac{3}{4\pi N_D}}. \tag{4}$$

The data obtained from the energetic blue shift of the DA transition are plotted in Fig. 11 as full black squares. From Hall effect measurements, the electron concentrations of the degenerate layers are taken as the donor concentrations (full green triangles) and from TOF-SIMS measurements, germanium concentrations are determined by means of the calibration discussed in Sec. III A (full blue circles).

In the range of medium doping, the measured donor concentrations are in good agreement with the trend of the vapor pressure curve. However, for the two highest doped layers, a deviation to lower concentrations is observed by SIMS, PL, and Hall effect measurements indicating that less Ge may be supplied for incorporation at high Ge cell temperatures. To check the amount of Ge supply, we measure the beam equivalent pressure (BEP_{Ge}) in our MBE system (full pink diamonds). In the range of high Ge effusion cell temperature, the measured BEP_{Ge} does not follow the vapor pressure curve anymore and shows the same temperature dependency as the experimental data for Ge incorporation. Therefore, we conclude that the incorporated Ge is determined by the supplied Ge atoms from the effusion cell. Up to now, it is unclear why the BEP_{Ge} does not comply with the vapor pressure curve. Unfortunately, in our system, the BEP_{Ge} cannot be measured for Ge cell temperatures lower than 900 °C.

The Ge concentrations measured by TOF-SIMS and the measured free electron densities agree within the measurement error. Therefore, nearly all of the incorporated Ge atoms are electrically active donors.

In the low doping range, a significant deviation of donor concentrations measured by TOF-SIMS and PL is observed, and the values deviate from the trend of the vapor pressure curve. The donor concentrations of the two lowest doped layers measured by PL show that the Ge concentration is equal to or lower than the level of residual doping. The Ge concentrations of the two lowest doped layers measured by TOF-SIMS imply that the Ge concentration in these layers is several orders of magnitude higher than expected by extrapolating with help of the vapor pressure curve. It is unclear if these values are reliable, although the GeN^- signals were higher than the noise level (blue dashed horizontal line). Further work is required to investigate the discrepancy between these values measured by different methods.

IV. SUMMARY

Germanium-doped cubic GaN layers with a nominal thickness of 600 nm were grown by plasma-assisted molecular beam epitaxy. Ge concentrations over several orders of magnitude up to 3.7×10^{20} cm^{-3} could be achieved. The incorporation of germanium into the c-GaN layers could be verified by time-of-flight secondary ion mass spectrometry. For comparison, additional silicon-doped c-GaN layers with doping levels up to 3.8×10^{19} cm^{-3} were grown. High-resolution x-ray diffraction measurements were carried out to estimate the dislocation densities of the layers. Doping up to the 10^{18} cm^{-3} range did not increase the formation of dislocations for both germanium and silicon dopants. Electrical properties were determined by Hall effect measurements. Germanium-doped layers feature an approximately 20% higher electron mobility than silicon-doped layers. A comparison of 13 K photoluminescence spectra of two similarly germanium- or silicon-doped layers reveals that the luminescence intensity is equal for both dopants, but the silicon-

Published under license by AIP Publishing.

doped layer shows a spectrally slightly narrower luminescence. The measured donor concentrations in our germanium-doped layers were compared to the trend of the vapor pressure curve of germanium. The donor concentrations follow the vapor pressure curve very well in the medium doping regime. In the range of low doping, the donor concentrations measured by different methods deviate from each other. In conclusion, doping with germanium and silicon results in comparable structural properties of the layers, but germanium doped layers exhibit better electrical properties.

ACKNOWLEDGMENTS

This work was financially supported by the Deutsche Forschungsgemeinschaft (DFG, German Research Foundation) - Projektnummer 231447078 - TRR 142 (via project B02).

REFERENCES

[1]D. J. As, Defect Diffus. Forum **206–207**, 87 (2002).
[2]R. E. L. Powell, S. V. Novikov, C. T. Foxon, A. V. Akimov, and A. J. Kent, Phys. Status Solidi C **11**, 385 (2014).
[3]E. Martinez-Guerrero, B. Daudin, G. Feuillet, H. Mariette, Y. Genuist, S. Fanget, A. Philippe, C. Dubois, C. Bru-Chevallier, G. Guillot, P. Aboughe Nze, T. Chassagne, Y. Monteil, H. Gamez-Cuatzin, and J. Tardy, Mat. Sci. Eng. B **82**, 59 (2001).
[4]Z. Q. Li, H. Chen, H. F. Liu, L. Wan, M. H. Zhang, Q. Huang, J. M. Zhou, N. Yang, K. Tao, Y. J. Han, and Y. Luo, Appl. Phys. Lett **76**, 3765 (2000).
[5]L. T. Romano, C. G. Van de Walle, B. S. Krusor, R. Lau, J. Ho, T. Schmidt, J. W. Ager III, W. Götz, and R. S. Kern, Physica B **273–274**, 50 (1999).
[6]S. Fritze, A. Dadgar, H. Witte, M. Bügler, A. Rohrbeck, J. Bläsing, A. Hoffmann, and A. Krost, Appl. Phys. Lett. **100**, 122104 (2012).
[7]M. Deppe, J. W. Gerlach, D. Reuter, and D. J. As, Phys. Status Solidi B **254**, 1600700 (2017).
[8]D. J. As, M. Deppe, J. W. Gerlach, and D. Reuter, MRS Adv. **2**, 283 (2017).
[9]J. Schörmann, S. Potthast, D. J. As, and K. Lischka, Appl. Phys. Lett. **90**, 041918 (2007).
[10]"Germanium (Ge), heats of fusion and sublimation, enthalpy and entropy, vapor pressure," in *Landolt-Börnstein, Group III*, edited by O. Madelung, U. Rössler, and M. Schulz (Springer-Verlag, Berlin, 2002), Vol. 41, Subvol. A1b, Online Document 533, p. 1
[11]P. D. Desai, J. Phys. Chem. Ref. Data **15**, 967 (1986).
[12]J. Ziegler, J. Biersack, and M. Ziegler, see www.srim.org for "SRIM, the Stopping and Range of Ions in Matter" (2013).
[13]J. R. de Laeter, J. K. Böhlke, P. de Bièvre, H. Hidaka, H. S. Peiser, K. J. R. Rosman, and P. D. P. Taylor, Pure Appl. Chem. **75**, 683 (2003).
[14]C. G. Van de Walle and J. Neugebauer, J. Appl. Phys. **95**, 3851 (2004).
[15]T. Markurt, L. Lymperakis, J. Neugebauer, P. Drechsel, P. Stauss, T. Schulz, T. Remmele, V. Grillo, E. Rotunno, and M. Albrecht, Phys. Rev. Lett. **110**, 036103 (2013).
[16]M. Wieneke, H. Witte, K. Lange, M. Feneberg, A. Dadgar, J. Bläsing, R. Goldhahn, and A. Krost, Appl. Phys. Lett **103**, 012103 (2013).
[17]P. Gay, P. B. Hirsch, and A. Kelly, Acta Metall. **1**, 315 (1953).
[18]A. T. Blumenau, J. Elsner, R. Jones, M. I. Heggie, S. Öberg, T. Frauenheim, and P. R. Briddon, J. Phys. Condens. Matter **12**, 10223 (2000).
[19]I. Akasaki and H. Amano, in *Properties of Group III Nitrides*, edited by J. H. Edgar, (INSPEC, London, 1994), p. 30.
[20]J. E. Ayers, J. Appl. Phys. **78**, 3724 (1995).
[21]D. J. As and K. Lischka, in *Molecular Beam Epitaxy: From Research to Mass Production*, edited by M. Henini (Elsevier, Amsterdam, 2013), p. 206.
[22]Z. X. Qin, H. Nagano, Y. Sugure, A. W. Jia, M. Kobayashi, Y. Kato, A. Yoshikawa, and K. Takahashi, J. Cryst. Growth **189/190**, 425 (1998).
[23]R. M. Kemper, T. Schupp, M. Häberlen, T. Niendorf, H.-J. Maier, A. Dempewolf, F. Bertram, J. Christen, R. Kirste, A. Hoffmann, J. Lindner, and D. J. As, J. Appl. Phys. **110**, 123512 (2011).
[24]A. F. Wright and U. Grossner, Appl. Phys. Lett. **73**, 2751 (1998).
[25]S. Dhar and S. Ghosh, J. Appl. Phys. **86**, 2668 (1999).
[26]M. Feneberg, M. Röppischer, C. Cobet, N. Esser, J. Schörmann, T. Schupp, D. J. As, F. Hörich, J. Bläsing, A. Krost, and R. Goldhahn, Phys. Rev. B **85**, 155207 (2012).
[27]G. Ramirez-Flores, H. Navarro-Contreras, A. Lastras-Martinez, R. C. Powell, and J. E. Greene, Phys. Rev. B **50**, 8433 (1994).
[28]D. J. As, F. Schmilgus, C. Wang, B. Schöttker, D. Schikora, and K. Lischka, Appl. Phys. Lett. **70**, 1311 (1997).
[29]J. Menniger, U. Jahn, O. Brandt, H. Yang, and K. Ploog, Phys. Rev. B **53**, 1881 (1996).
[30]D. J. As, U. Köhler, M. Lübbers, J. Mimkes, and K. Lischka, Phys. Status Solidi A **188**(2), 699 (2001).
[31]D. K. Schroder, *Semiconductor Material and Device Characterization* (John Wiley & Sons, Inc., Hoboken, 2006), p. 606.
[32]G. W. Thomson, Chem. Rev. **38**, 1 (1946).

Published under license by AIP Publishing.